Eur. Radiol. 9, 1775–1780 (1999) 

European
Radiology

*Technical note*

# Three-dimensional MR angiography of a nitinol-based abdominal aortic stent graft: assessment of heating and imaging characteristics

**P. R. Hilfiker, H. H. Quick, T. Pfammatter, M. Schmidt, J. F. Debatin**

Institute of Diagnostic Radiology, University Hospital Zurich, Rämistrasse 100, CH-8091 Zurich, Switzerland

Received: 24 August 1998; Revised: 10 December 1998; Accepted: 2 April 1999

**Abstract.** Objective: To assess heating- and 3D MRA imaging characteristics of a commonly used aortic stent graft in a 1.5T MR-environment. Materials and methods: A bifurcated stent graft (Vanguard; Boston Scientific, Oakland, N.J.) was evaluated in vitro regarding localized heating effects as well as imaging appearance using fast 3D GRE sequences. To quantitate stent related artifacts, stent wall thickness and luminal diameters were measured. Subsequently eight patients were imaged three months following placement of an aortic stentgraft with 3D MRA. Images were assessed for the presence of stent leaks, luminal patency, and stent configuration. Results: There were no temperature changes associated with the stent during scanning. Wall thickness measurements overestimated true stent thickness, resulting in minimal underestimation of luminal diameters on 3D MRA images. In vivo imaging confirmed these results. Stent patency was confirmed in all 8 patients. Conclusion: Contrast-enhanced 3D MRA appears well suited for the evaluation of the abdominal and pelvic vasculature following aortic implantation of a Vanguard stent.

**Key words:** MR imaging – Artifact – Vascular studies – Safety – Grafts – Interventional procedure – Stents and prosthesis

## Introduction

Based on encouraging initial data, percutaneous stent grafting is increasingly employed as a less-invasive alternative for the treatment of infrarenal abdominal aortic aneurysms [1]. The covered stent is placed within the aorta in an attempt to exclude the aneurysm. The long-term success of this endoluminal procedure is predicated upon the availability of accurate imaging data during, as well as before and following, the procedure.

Pre-procedural planning can be based on either 3D CT- or 3D MR angiography. The data sets permit detailed morphologic analysis of the aneurysm itself as well as assessment of possible branch vessel involvement. In contrast to surgery, aneurysmal stenting requires long-term imaging follow-up [2]. Whereas several techniques, including duplex ultrasound, digital subtraction angiography (DSA), and CTA, have been employed for this purpose [2], the expectation of severe stent-induced artifacts and safety concerns have prevented 3D MRA from being used widely [3].

The purpose of this study was to assess heating effects as part of safety review of the most commonly used aortic stent in the 1.5-T MR environment and to evaluate its effect onto 3D MRA image quality. The extent of artifacts and their impact on stent-related measurements was assessed with in vitro experiments and compared to those seen in vivo.

## Materials and methods

### *Stent graft*

Experiments were performed on a stent graft, used routinely in our institution (Vanguard, Boston Scientific, Oakland, N.J.). This particular stent graft is approved by the regulatory agencies and is commercially available in Europe. It is a self-expanding endoprosthesis composed of a nitinol frame annealed into a tubular zigzag configuration by a 7–0 polypropylene thread [4] and covered with a 0.1-mm woven-polyester fabric. The bifurcated device has two components which are joined intraluminally: the larger component consists of an aortic graft with a short, 10-mm-wide iliac branch, into which the smaller component is inserted [5]. Both ends of the stent frame, as well as the junction between the two sections, are tagged with a platinum marker allow-

*Correspondence to:* J.F. Debatin, Dept. of Diagnostic Radiology, University Hospital Essen, Hufelandstr. 55, D-45122 Essen, Germany

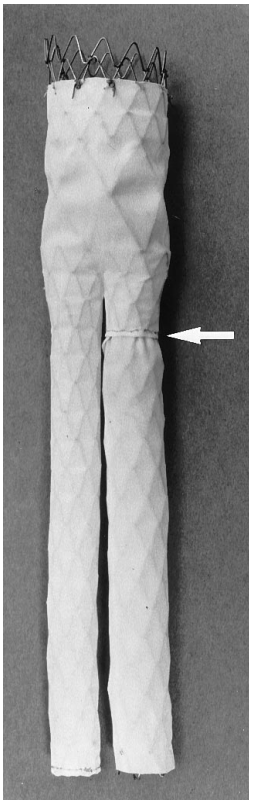

**Fig. 1.** Stent graft used for the endoluminal treatment of infrarenal aortic aneurysms (Vanguard, Boston Scientific, Oakland, N.J.). The graft has two components that are inserted separately and subsequently joined: the primary component consists of an aortic and iliac stent graft with an attachment site for the secondary component, which is placed in the contralateral iliac artery. Junction of the two stent components *(arrow)*

ing proper device positioning under fluoroscopic guidance. For in vitro experiments, a 153-mm-long model with an aortic diameter of 24 and an iliac diameter of 10 and 12 mm was used (Fig. 1).

All MR imaging was performed on a 1.5-T MR scanner (Signa EchoSpeed, General Electric Medical Systems, Milwaukee, Wis.) using an anteroposterior phased-array surface coil for signal reception.

*In vitro stent imaging*

The inflated stent graft was embedded into agar-gel and placed in the isocenter of the scanner with its long axis parallel to the $B_0$ field. To simulate the intraluminal aortic signal during 3D MRA, the gel was spiked with 0.025 M Gd-DTPA (Magnevist, Schering, Berlin, Germany). Based on axial multiphase gradient-recalled-echo (GRE) localizing images, 3D Fourier transform fast spoiled GRE images were acquired which consisted of 44 contiguous 2.5-mm coronal sections. The sequence employs a sampling bandwidth of ± 62.5 kHz, a TR/TE of 4.0/1.9 ms, and a flip angle of 40°. Combined with a 24 × 24-cm field of view (FOV), a 256 × 192 matrix provided an in-plane resolution of 0.9 × 1.2 mm. Stent wall thickness and diameters were measured on axial reconstructions at five locations:

1. Proximal aortic portion traversing the platinum marker
2. Center of the aortic portion
3. Proximal iliac portion traversing the platinum marker
4. Center portion of the iliac legs
5. Distal iliac portion traversing the platinum marker

On each stent, wall thickness was measured at four points, each spaced 90° from one another. At each location, two orthogonal luminal diameters, each connecting two opposite points, were also measured. Measurements were based on signal intensity plots drawn orthogonal to the tangent of each measurement point in order to avoid errors arising from varying window/level settings. Based on this signal intensity curve, the luminal stent diameter was defined as the distance between the two inner points of half maximum signal intensity. Wall thickness was defined as the distance between the inner and the outer point of half maximum signal intensity.

*In vitro stent heating*

To assess the degree of localized heating, three probes of a fluoroptic thermometer (Luxtron 790, Santa Clara, Calif.) were placed onto the gel-embedded stent graft: one at each end, and one at the junction of the two stent graft components. The temperature was monitored continuously at a rate of four updates per second from all three sites during repeated scanning (up to 4 min) with the above-outlined 3D fast spoiled GRE sequence. Beyond maximizing the transmit gain (TG), all parameters were identical to those described above.

*In vivo stent imaging*

Eight patients (all men; mean age 68.2 years) who had been treated with a bifurcated stent graft (Vanguard, Boston Scientific, Oakland, N.J.) for an infrarenal abdominal aortic aneurysm underwent MR imaging 3 months following placement of the bifurcated stent graft. After providing informed consent, a contrast-enhanced 3D MRA data set using the following parameters was acquired: TR/TE 4.0/1.9 ms, flip angle 40°, field of view 40 × 30 cm, matrix 256 × 192. Using partial k-space sampling, 44 contiguous 2.5-mm sections were collected in the coronal plane breath-held over 28 s. A test bolus technique [6] was employed to determine the proper scan delay. The 3D MRA data set was acquired following the intravenous bolus injection of Gd-DTPA at a dose of 0.2 mmol/kg. The agent was administered at a rate of 2.5 ml/s using an automated injector (MR Spectris, Medrad, Philadelphia, Pa.). Multiplanar reformations, allowing cross sectional analysis of the 3D data set in any desired plane, were rendered of the aorta and its branches, along with subvolume (targeted) and entire-volume maximum intensity projection images. The 3D MRA images were assessed for the presence of endoleaks, luminal patency in the stent graft, and overall stent configuration. As routine procedure after stent implantation, all patients also underwent spiral CT.

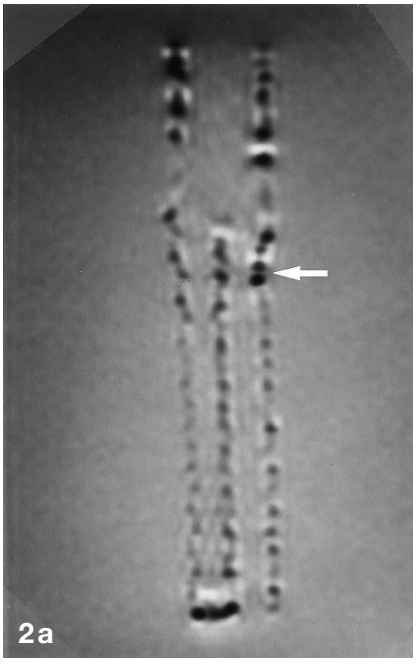


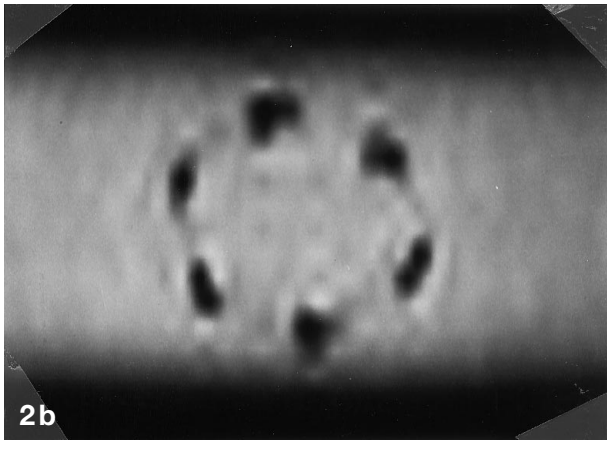


**Fig. 2 a, b.** In vitro 3D MRA of the stent graft. **a** The woven wires of the stent graft are well visualized on the coronal source image against the contrast enhanced Agar gel. Platinum markers are at the junction of the two stent components *(arrow)*. **b** Axial reconstruction through the center of the stent depicts the stent as a dark ring

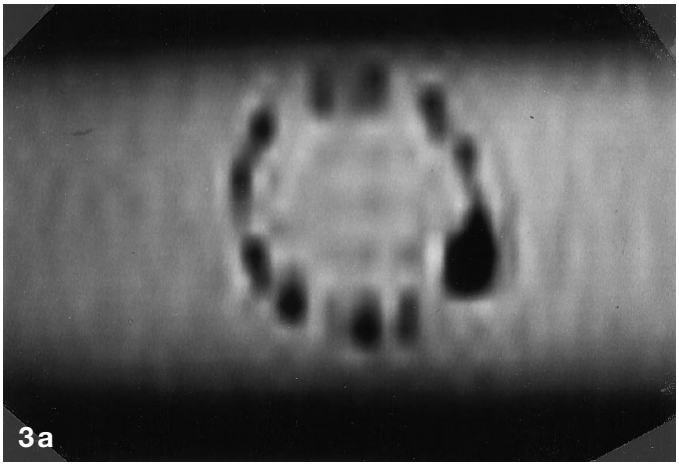


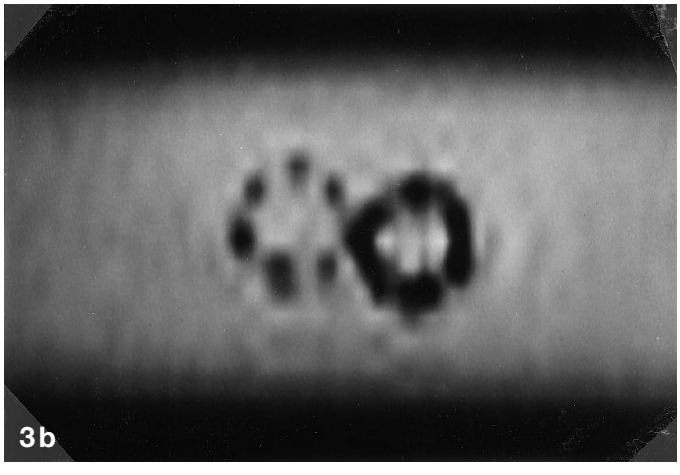


**Fig. 3 a, b.** Axial reconstructions traversing the platinum marker at **a** the proximal aortic portion and **b** the platinum marker at the junction of the two stent components in the proximal iliac portion. The platinum-induced signal voids simulate a widening of the stent wall on MR images and may simulate a stenosis at the junction at the two stent components

## Results

No temperature changes were recorded even after 4 min of continuous 3D GRE scanning using the highest possible TG. The stent graft was well delineated on MR images. The stent structure created a signal void and was thus displayed as a dark ring. The low level of artifact on the 3D GRE images allowed the woven wires of the stent graft to be visualized against the contrast-enhanced agar gel (Fig. 2). The 0.1-mm woven-polyester fabric could not be delineated. Platinum markers exhibited artifacts, inducing a focally enlarged signal void (Fig. 3).

Wall thickness measurements at the five locations of the stent graft overestimated true thickness, resulting in a slight underestimation of luminal stent diameters (Table 1). Wall thickness measurements obtained at the junction of the two stent components in the proximal portion of one iliac leg revealed a wider appearance due to the overlap of the platinum markers (Fig. 3; Table 1).

All eight patients tolerated the MR exam well, and were able to fully comply with the 28-s breath-hold interval. Despite considerable variation in vascular morphology, the imaging volume contained the targeted vascular territory, encompassing the entire longitudinal extent of the stent graft, the renal arteries, and the pelvic arterial system. Both the metallic filaments and the markers were identifiable (Fig. 4). The contrast-enhanced aortic lumen within the stent was well visualized, thereby documenting stent-graft patency. Confirmed by CTA there was no evidence of an endoleak in any of the evaluated patients on the 3D MRA data sets.

A stent deformity in the distal right iliac leg was evident on the 3D MRA images in one patient. The finding was confirmed by CTA and later by catheter angiography and treated by implanting a non-covered self-expandable stent (Easy Wallstent, Schneider Worldwide, Bülach, Switzerland; Fig. 5).

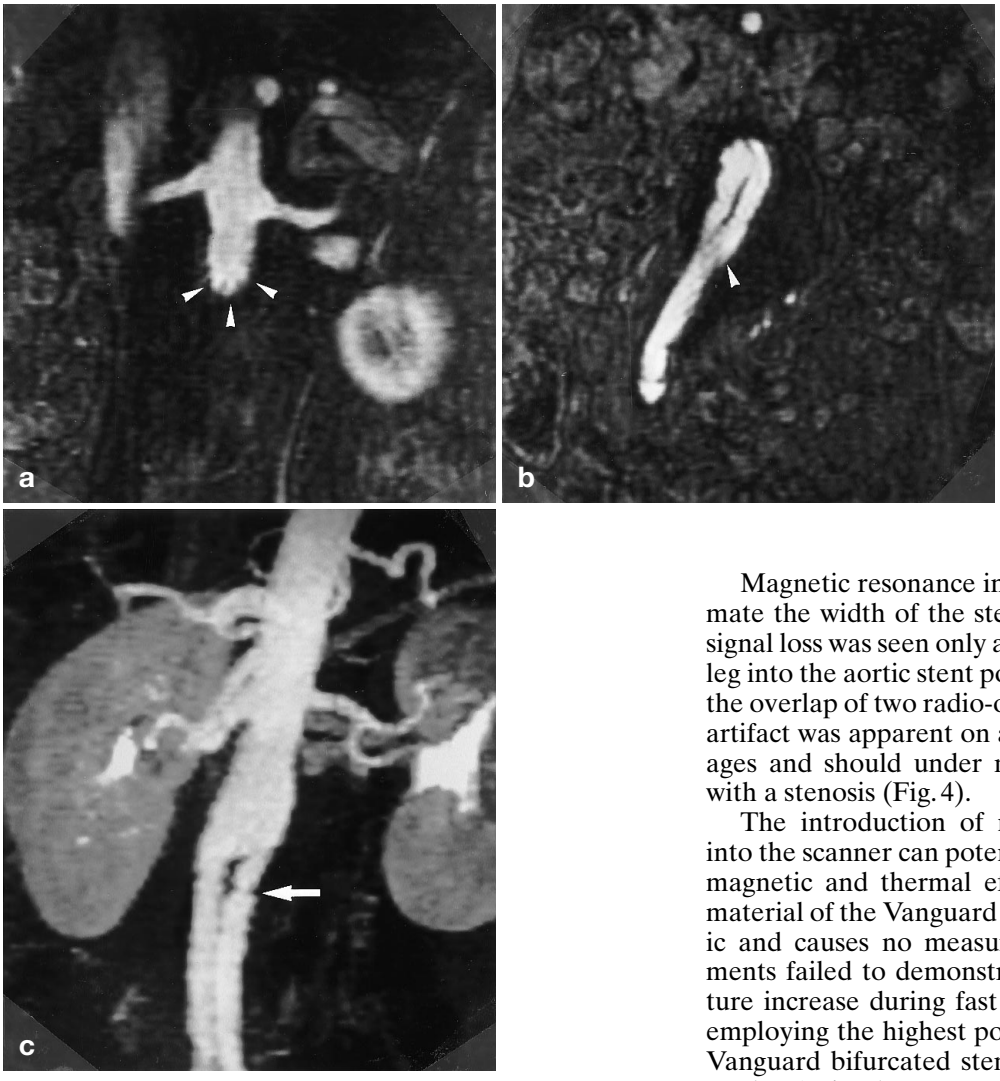


**Fig. 4. a, b** Source and **c** maximum-intensity-projection images of a coronal 3D MRA data set acquired in a patient 3 months following aortic stent grafting. The stent filaments are well delineated in both aortic **(a)** and iliac **(b)** segments in vivo on the coronal source images *(arrowheads)*. The overlap of platinum markers at the junction of the two stent components in the proximal right iliac artery causes a widened signal void *(arrow)*, which should not be confused with a stenosis **(c)**

## Discussion

Three-dimensional MRA is widely used in the pre-therapeutic work-up of patients with abdominal aortic aneurysms [3]. For fear of severe stent-related artifacts, the technique has, however, not been routinely used for post-stenting follow-up studies [3], except in one recently published clinical study by Engellau et al. [7] (mainly with a different device). The results of the presented in vitro and in vivo experiments show these concerns to be unfounded. The very short echo time of less than 2 ms, inherent to the fast 3D GRE acquisition, limits stent-related magnetic susceptibility artifacts. The nitinol frame filaments of the stent graft are identifiable on the individual sections and reformations as distinct areas of signal void.

Magnetic resonance images tend to slightly overestimate the width of the stent-graft wall. A wider area of signal loss was seen only at the insertion of the iliac stent leg into the aortic stent portion. This most likely reflects the overlap of two radio-opaque platinum markers. This artifact was apparent on all in vitro and in vivo MR images and should under no circumstances be confused with a stenosis (Fig. 4).

The introduction of metallic conducting materials into the scanner can potentially lead to hazardous ferromagnetic and thermal effects. Nitinol, the underlying material of the Vanguard stent graft, is not ferromagnetic and causes no measurable torque [8]. Our experiments failed to demonstrate any appreciable temperature increase during fast 3D GRE imaging even while employing the highest possible transmit gain. Thus, the Vanguard bifurcated stent graft can indeed be considered safe in the MR environment, without incurring the risk of magnetically induced device migration or tissue heating.

**Table 1.** Measurement of wall thickness and diameters. The stent graft had the following sizes: 24-mm diameter of the aortic part; 10-mm diameter of the attached iliac section; 10-mm diameter of the inserted iliac section at the junction and 12 mm at the free end

| | MRI (mm) | Stent dimensions (mm) |
|---|---|---|
| ∅ Proximal aortic part | 21.8 ± 0.7 | 24 |
| ∅ Center of aortic part | 21.7 ± 0.6 | 24 |
| ∅ Proximal iliac portion | | |
| Attached iliac section | 7.6 ± 1.1 | 10 |
| Inserted iliac section | 5.5 ± 0.8 | 10 (junction) |
| ∅ Center of iliac legs | | |
| Attached iliac section | 7.7 ± 1.0 | 10 |
| Inserted iliac section | 9.2 ± 1.0 | 12 |
| ∅ Distal iliac legs | | |
| Attached iliac section | 7.6 ± 0.9 | 10 |
| Inserted iliac section | 8.5 ± 0.6 | 12 |
| Wall thickness[a] | 2.4 ± 0.8 | 0.35 |
| Platinum markers | 3.4 ± 1.3 | 0.95 |

[a]Without platinum markers

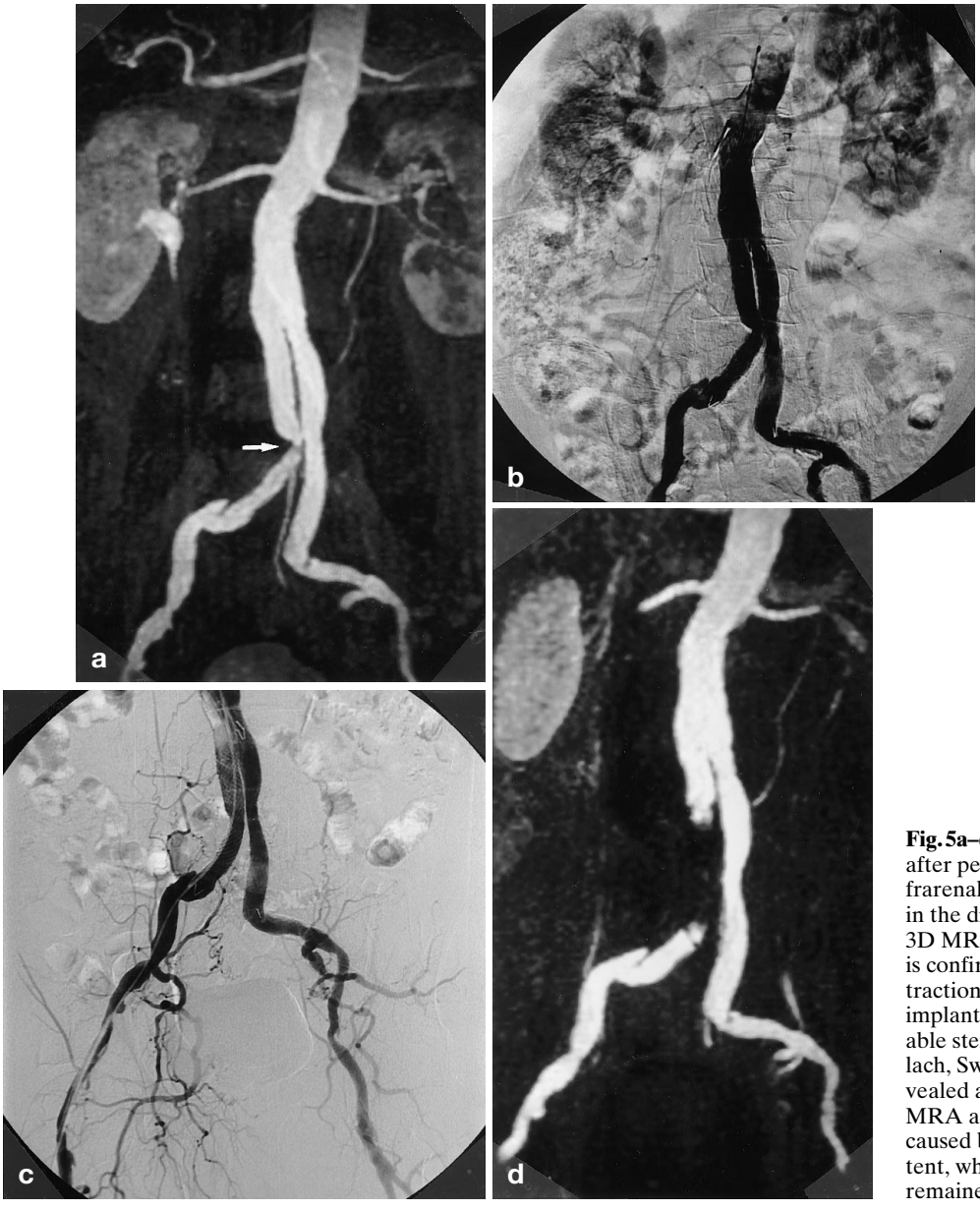


**Fig. 5a–d.** A 71-year-old patient 3 months after percutaneous stent grafting of an infrarenal aortic aneurysm. **a** Stent deformity in the distal right iliac leg is evident on the 3D MRA image set *(arrow)*. **b** The finding is confirmed by intra-arterial digital subtraction angiography (DSA). **c** Following implantation of a non-covered self-expandable stent (Easy Wallstent, Schneider, Bülach, Switzerland) the intra-arterial DSA revealed a good result. **d** Subsequent 3D MRA acquisition depicts a large signal void caused by the additionally implanted Wallstent, whereas the lumen of the aortic stent remained well visible

After dispelling artifact- and safety-related concerns for this particular stenting device, the potential advantages of 3D MRA regarding its application to post-stent follow-up imaging can be considered. Beyond the absence of ionizing radiation, paramagnetic contrast agents are not nephrotoxic [9], permitting their repetitive use even in patients with impaired renal function. As many of the patients with aortic aneurysms have concomitant renal insufficiency [10], this aspect is of particular significance. It is, however, crucial to point out that the favorable results documented with the Vanguard bifurcated stent graft cannot be generalized to other devices. Both artifact and safety characteristics are dependent on the composition of the individual stent graft and on the field strength of the MR system.

In conclusion, contrast-enhanced 3D MRA appears well suited for assessing the abdominal and pelvic vasculature following aortic stent implantation. The evaluated device exhibited neither ferromagnetism nor heating at 1.5 T during scanning. In this limited preliminary study, 3D MRA images were found to permit a comprehensive assessment of the arterial lumen, as well as perivascular tissues. Provided these results can be confirmed in larger series, 3D MRA may well evolve into an attractive alternative for the follow-up of stent-grafting procedures. A focal area of artifactual signal loss at the insertion of the iliac stent leg into the aortic stent component should not be confused with a stenosis.

## References

1. Blum U, Voshage G, Lammer J et al. (1997) Endoluminal stent-grafts for infrarenal abdominal aortic aneurysms. N Engl J Med 336: 13–20
2. Rozenblit A, Marin ML, Veith FJ, Cynamon J, Wahl SI, Bakal CW (1995) Endovascular repair of abdominal aortic aneurysm:

value of postoperative follow-up with helical CT. Am J Roentgenol 165: 1473–1479
3. Thurnher SA, Dorffner R, Thurnher MM et al. (1997) Evaluation of abdominal aortic aneurysm for stent-graft placement: comparison of gadolinium-enhanced MR angiography versus helical CT angiography and digital subtraction angiography. Radiology 205: 341–352
4. Cragg AH, De Jong SC, Barnhart WH, Landas SK, Smith TP (1993) Nitinol intravascular stent: results of preclinical evaluation. Radiology 189: 775–778
5. Blum U, Langer M, Spillner G et al. (1996) Abdominal aortic aneurysms: preliminary technical and clinical results with transfemoral placement of endovascular self-expanding stent grafts. Radiology 198: 25–31
6. Hany TF, McKinnon GC, Leung DA, Pfammatter T, Debatin JF (1997) Optimization of contrast timing for breath-hold three-dimensional MR angiography. J Magn Reson Imaging 7: 551–556
7. Engellau L, Larsson EM, Albrechtsson U et al. (1998) Magnetic resonance imaging and MR angiography of endoluminally treated abdominal aortic aneurysms. Eur J Vasc Endovasc Surg 15: 212–219
8. Laissy JP, Grand C, Matos C, Struyven J, Berger JF, Schouman-Claeys E (1995) Magnetic resonance angiography of intravascular endoprostheses: investigation of three devices. Cardiovasc Intervent Radiol 18: 360–366
9. Nelson KL, Gifford LM, Lauber-Huber C, Gross CA, Lasser TA (1995) Clinical safety of gadopentetate dimeglumine. Radiology 196: 439–443
10. Muluk SC, Painter L, Sile S et al. (1997) Utility of clinical pathway and prospective case management to achieve cost and hospital stay reduction for aortic aneurysm surgery at a tertiary care hospital. J Vasc Surg 25: 84–93

# Book reviews

European Radiology

**Thiel W.: Photographic atlas of practical anatomy. I. Abdomen, lower limb.** Berlin Heidelberg New York: Springer, 1997, 844 pages, 414 figures, DM 498.00, ISBN 3-540-61195-9

This atlas is published in two two-volume sets. The first set deals with the abdomen and lower limb and is discussed here. The second set deals with head, neck, back, chest and upper extremities and was not reviewed.

The first of the two volumes is a colour atlas containing colour images of gross anatomical structures. In the brief descriptions that accompany the colour images, all important structures are named and boldfaced for emphasis. The second volume is a companion book with correlative black-and-white photographs that are marked with arrowheads. Numbers in the margins line up with these symbols and are keyed to a list of anatomical terms (in English).

The quality of both colour and black-and-white photographs is superb. Anatomical regions are very well dissected and three-dimensional anatomy is nicely shown. Cross-sectional views are not included because, according to the authors, 'an appreciation of cross-sectional anatomy will follow automatically from an understanding of three-dimensional anatomy'.

In conclusion, this is a high-quality atlas with superb photographs showing three-dimensional anatomy in a way that can be applied directly to surgical patients. The books will be of great value for surgeons and anatomists, students or teachers. However, the radiologist will view the absence of cross-sectional views as a shortcoming. J. Verschakelen, Leuven

**Mukherji S. K., Castelijns J. A. (Editors): Modern head and neck imaging.** Berlin Heidelberg New York: Springer, 1999, 245 pages, 318 illustrations, DM 298.00, ISBN 3-540-62549-6

'Modern' in the title refers to the presentation of different techniques that have been introduced in the field of head and neck imaging in recent years. Fifteen chapters, written by more than 30 authors, are presented, dealing with items such as magnetization transfer imaging, MR-guided interventions and therapy, spectrosocpy, functional imaging, PET scanning and 3D imaging. The quality of the chapters is variable. In an interesting first chapter on magnetization transfer imaging of the extracranial head and neck it is emphasized that only the surface has been scratched of the value of this technique. In the fourth chapter, on spectroscopy, interesting ideas are formulated but the illustrations are somewhat confusing because of the use of different scales. Moreover there is some confusion on many occasions between fluid peaks and fat peaks. In the chapter on T2-weighted gradient echo imaging of the inner ear the images are of moderate quality. The chapter would be more comprehensive if more T1-weighted images after gadolinium administration had been included. Chapters 13 and 14 on 3D imaging are interesting but there is a lot of overlap. It is unclear to me why a chapter on dacryocystography is included in a book about recent to very recent imaging techniques.

The price of this book is acceptable for the quality of the images – which is overall good to excellent except for the chapter on the temporal bone. I would only recommend this book to radiologists who work or intend to work with advanced imaging modalities in the head and neck region. M. Lemmerling, Gent